

## Nested Bars and Associated Morphology of Central Kpc in Disk Galaxies

Isaac Shlosman<sup>1</sup>

*Joint Institute for Laboratory Astrophysics, Campus Box 440,  
University of Colorado, Boulder, CO 80309-0440, USA*

**Abstract.** We discuss different aspects of nested bar systems, both observational and theoretical. Such systems consist of a large-scale primary bar leading to the formation of a sub-kpc size secondary bar, whose pattern speed differs substantially from that of the main bar. Specifically, we focus on the origin and gravitational decoupling of nested bars, and their characteristic gas flows on scales of  $\sim 100$  pc–10 kpc, with and without gas gravity. We find that the gas response in nested bars differs profoundly from that in single bars, and that no offset dust lanes form in the secondary bars. We also discuss briefly the importance of nested bar systems for redshifts corresponding to galaxy formation epoch.

### 1. Introduction

The ‘barred’ branch dominates the Hubble’s fork. In the optical band, about 1/3 of all disk galaxies are strongly barred, and an equal fraction is designated as ‘intermediate barred’ (e.g., Sellwood & Wilkinson 1993). In the near-infrared (NIR), the majority of the disks, more than 2/3, appear to be barred (e.g., Mulchaey & Regan 1997; Knapen, Shlosman & Peletier 2000; Grosbol, these proceedings). The importance of bars stems from their decisive role in galactic dynamics: breaking the axial symmetry of host galaxies speeds up the dynamical and secular evolution in the disks. The influence of bars during the galaxy formation epoch, the part they play in coupling the disks to halo material and the evolution of bar fraction with redshift only recently have attracted attention.

Theoretical studies of bars have relied on the analysis of dominant families of stellar orbits supplemented by 2-D and 3-D numerical simulations of one- and two-component galactic disks embedded in ‘live’ or ‘frozen’ halos. The main effort has been directed towards understanding the intrinsic bar instability which leads to the radial mass redistribution as well as triggers and fuels the star formation in the disk, especially within the central kpc. The presence of *large-scale* bars is insufficient to maintain the nonstellar (AGN-type) activity within the central pc, and additional, most probably, dynamical factors are clearly necessary for this purpose (Shlosman, Begelman & Shlosman 1990).

---

<sup>1</sup>JILA Visiting Fellow. Permanent address: Department of Physics & Astronomy, University of Kentucky, Lexington, KY 40506-0055

Recent progress in ground-based instruments and the availability of the *HST* has allowed for the first time a meaningful analysis of central morphology and kinematics. Although our knowledge of the inner regions of disk galaxies is clearly incomplete, certain patterns in their dynamical evolution and their relationship to larger and smaller spatial scales have emerged.

At least dynamically, the inner parts of disk galaxies can be defined by the positions of the inner Lindblad resonances (ILRs), typically at about 1 kpc from the center. These resonances between the bar pattern speed and the precession rate of periodic orbits play an important role in filtering density waves, either stellar or gaseous, propagating between the bar corotation radius (CR) and the center. They are usually delineated by elevated star formation rates and the concentration of molecular gas in nuclear rings. These rings exhibit a rich morphology and can serve as cold gas reservoirs for fueling the central activity.

The resolved morphology of central kpc in barred galaxies has revealed additional grand-design spirals and bars. Defining nested bar systems as those with more than one bar, stellar or gaseous, we refer to large, kpc-scale bars as “primary,” while the sub-kpc bars as “secondary.” The theoretical rationale behind these definitions is that secondary bars are believed to form as a result of radial gas inflow along the large-scale bar and, therefore, are expected to be confined within the ILRs (Shlosman, Frank, & Begelman 1989). Below we review the properties of such nested bars and associated morphologies in disk galaxies, their dynamical states and the resulting gas flows on scales of  $\sim 100$  pc–10 kpc.

## 2. Nested Bars: Observations and Initial Statistics

By a simple analogy with the large-scale bars and their effect on the disk evolution, secondary bars are expected to dominate the dynamics inside the central kpc. Although the sub-kpc bars had been probably detected already by de Vaucouleurs (1974) and others as optical isophote twists in the central regions of barred galaxies, they have been interpreted as triaxial bulges. High resolution ground-based observations have revealed additional small bars residing within the large-scale stellar bars (Laine et al. 2002 and refs. therein).

While the first detections of sub-kpc bars were made in stellar light, these objects can contain arbitrary fractions of gas, and in extreme cases can be dynamically dominated by molecular gas, as evident from their detection in CO and the NIR lines of H<sub>2</sub> emission (e.g., Ishizuki et al. 1990; Devereux, Kenney, & Young 1992; Forbes et al. 1994; Mirabel et al. 1999; Kotilainen et al. 2000; Maiolino et al. 2000). CO observations have a rather low spatial resolution, but do allow the determination of the offset angle between the large stellar and the small gaseous bars. It is not yet clear whether stellar- and gas-dominated sub-kpc bars have a common origin or describe a concurrent phenomenon. In this section we focus on nested stellar bars, as seen in NIR and optical starlight. Statistical properties of gaseous bars cannot be analyzed at present.

Embedded nuclear bars have been detected with the *HST* (e.g., Martini & Pogge 1999; Regan & Mulchaey 1999). The largest sample (112) of disk (S0-Sc) galaxies analyzed so far to infer statistical properties of nested bars in general, and in Seyferts and non-Seyferts in particular, is that of Laine et al. (2002). The Seyfert sample consists of most of the objects in the local universe ( $v_{\text{hel}} < 6000$

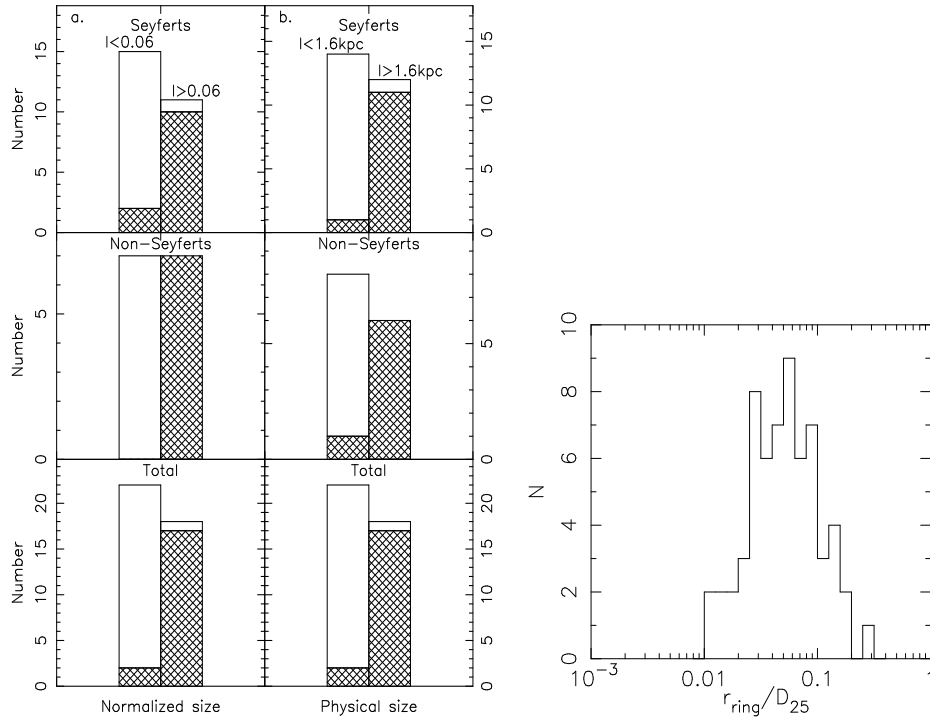
km s<sup>-1</sup>) observed with NICMOS, with the addition of a few well-known objects. Highly inclined galaxies have been removed. But, unless the interaction has been accompanied by a strong morphological distortion, interacting galaxies have not been discarded. The Seyfert sample consisted of 56 objects and was matched by a control sample of 56 NICMOS non-Seyferts, in absolute  $B$  magnitude, distance, axis ratio and morphological type. Ground-based data has been used for the outer disks. To classify a galaxy as barred, criteria set in Knapen et al. (2000) have been applied. Note, that this strictly conservative approach which was not ‘curved’ will lead to lower limits in the bar detection.

Laine et al. (2002) results have confirmed a substantial fraction of nested bars in disk galaxies, probably in excess of 20–25%, and that about 1/3 of barred galaxies host second bar. The observed nested bars in Seyferts and non-Seyferts have revealed an intriguing property — the existence of a critical physical length,  $l_{crit} \approx 1.6$  kpc, which separates the primary and the secondary bars, resulting in a clear bimodal size distribution with only little overlap (Fig. 1b). When the bar sizes are normalized to those of the respective host galaxies,  $D_{25}$ , the overlap between the two bar species is further reduced and  $l_{crit} \approx 0.06$  (Fig. 1a). Both critical sizes appear to be mutually consistent because the primary bar lengths exhibit a roughly linear correlation with the parent galaxy sizes, while the secondary bar lengths are *independent* from the sizes of their host galaxies (Fig. 7 in Laine et al.). The importance of this result can be inferred from the fact that only in this case the normalized bar lengths will preserve the identity of both bar groups and there will be no further mixing between the primary and secondary bars in the normalized size space. If, for example, both types have had a linear correlation with  $D_{25}$  with non-zero slopes, the two bar groups would be separated in physical but mixed in the normalized space. This is the first time that such a clear separation of primary and secondary bar lengths has been shown observationally. Because the samples include all the Hubble types from S0 to Sc, the minimal overlap between the two bar classes means that this result stands regardless of the morphological class of the galaxy.

A simple explanation for a bimodal distribution of bar sizes can be put forward. The linear correlation of the primary bar with galaxy size means that bars extend to a fixed number of radial scalelengths in the disk (see also Athanassoula & Martinet 1980; Martin 1995). The absence of such a correlation for the secondary bars, together with their limited range of sizes, hints to a different physical nature of formation and dynamics compared to the primary bars.

Numerical simulations of nested bars show that the secondary bars are confined to within the ILRs of the primary bars. The outer ILR develops close to the radius of velocity turnover, or more basically, where the mass distribution in the inner galaxy switches from 3D to 2D,  $\sim 1$ –2 kpc is a reasonable estimate. For the early Hubble type galaxies (S0-Sb), this leads to the appearance of an ILR at about the bulge radius. For the later Hubble type galaxies or early types with small bulges, the height of the disk becomes comparable to the radius of the disk at a point where the 2D disk approximation breaks down.

If primary and secondary bars had a similar evolutionary history, one should expect a linear correlation between the secondary bar length and  $D_{25}$ , because of the observed correlations between the disk, large-scale bar, and bulge sizes. However this correlation is clearly ruled out by the present data. Large-scale



*Left:* Figure 1. Distribution of normalized (a) and physical (b) primary (cross-hatched) and secondary (blank) bar sizes. The top panels show Seyferts, the middle panels non-Seyferts, and the bottom panels display the totals. The bar lengths,  $l$ , were normalized by the host galaxy diameter  $D_{25}$  and the resulting values were divided into two groups,  $l < l_{\text{crit}} = 0.06$  and  $l > l_{\text{crit}} = 0.06$ . In physical units  $l_{\text{crit}} = 1.6$  kpc. The lengths  $l_{\text{crit}}$  were chosen to minimize the overlap between the two groups. *Right:* Figure 2. Distribution of normalized nuclear ring diameters. Data were mostly taken from Buta & Crocker (1993), with addition of a few “famous” nuclear ring galaxies (Laine et al. 2002).

bars are also known to extend just short of their CR, based on the shapes of their offset dust lanes (Athanasoula 1992). However, the *secondary* bars are not expected to follow this rule or to possess offset dust lanes (Shlosman 2001; Shlosman & Heller 2002; Maciejewski et al. 2002). As discussed in section 3, they must be short of their CR. This property of secondary bars is expected to destroy any correlation between their size and that of the parent galaxy.

Laine et al. (2002) have compiled a sample of 62 galaxies with nuclear rings (mostly from Buta & Crocker 1993) and determined their normalized size distribution (Fig. 2). It peaks at  $r_{\text{ring}}/D_{25} = 0.06$ , further supporting the view that the value 0.06 acts as the dynamical separator between secondary and primary bars. This result is consistent with the secondary bars being limited by the size of the ILR, since nuclear rings are associated with the ILRs.

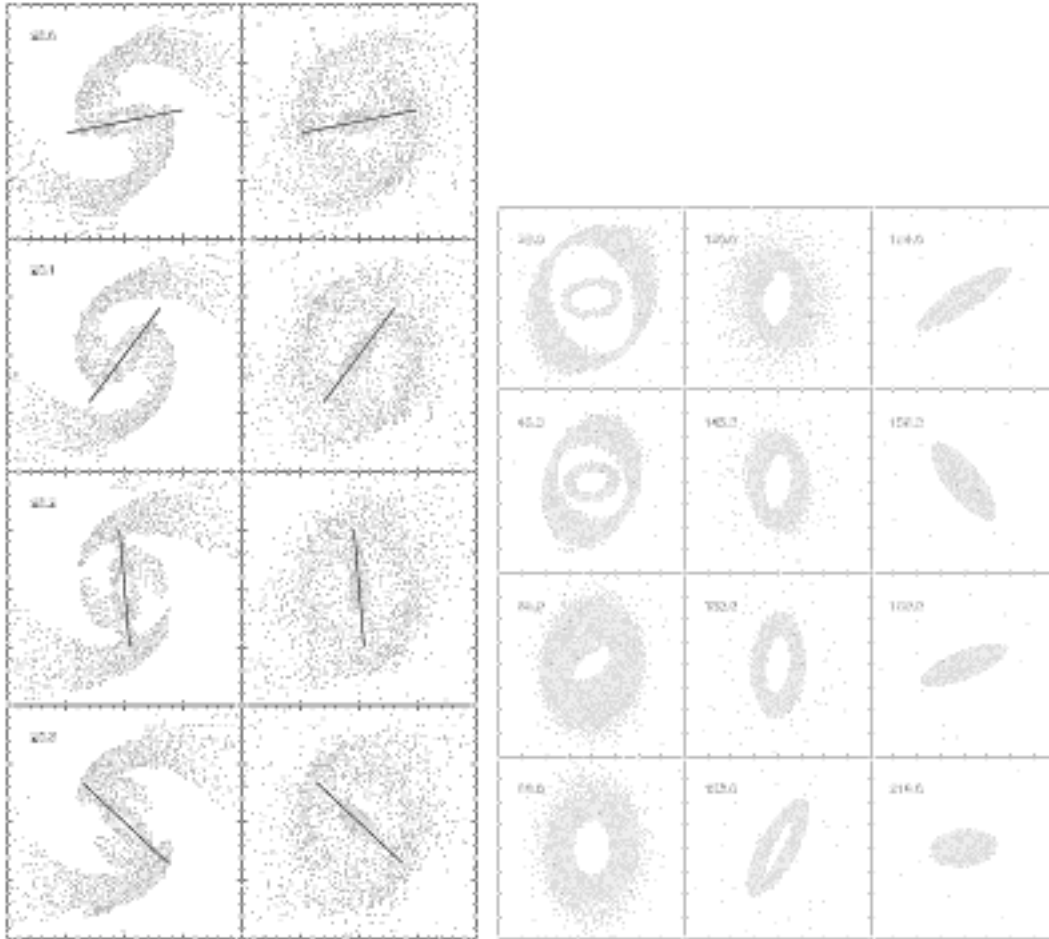
To summarize: (i) nested bars exhibit a bimodal size distribution with a possibility that ILRs serve as dynamical separators between primary and sec-

ondary bars; *(ii)* single and primary bars show a correlation between the ellipticity and the bar length. This result is extended here for galaxies from S0 to Sc; *(iii)* only few *single* bars appear shorter than  $l_{crit} = 0.06$ . Single bars also have higher average ellipticities than nested bars, and a different distribution in morphological types; *(iv)* Seyferts have an excess of bars,  $73\% \pm 6\%$  of Seyferts have at least one bar, against only  $50\% \pm 7\%$  of non-Seyferts. The statistical significance of this is at the  $2.5\sigma$  level, and strengthens the result of Knapen et al. (2000) which was based on smaller samples. Overall it seems that NIR isophote fitting shows difficulties when applied to sub-kpc bars, resulting from localized and distributed sites of dust extinction and bright stars within the central kpc, leading to a substantial underestimate of bar fraction.

### 3. Gas Response in Nested Bar Systems

Observational studies of secondary bars customarily assume that their properties, e.g., gas dynamics and appearance of characteristic offset dust lanes, are identical to those of large-scale bars (e.g., Martini & Pogge 1999; Regan & Mulchaey 1999). Theoretically, gas response to the double bar torquing has been only recently analyzed, when the pattern speed of the secondary bar,  $\Omega_s$  substantially exceeds that of the primary bar,  $\Omega_p$  (Shlosman 2001; Shlosman & Heller 2002; Maciejewski et al. 2002). These simulations and general theoretical considerations support the view that secondary bars are not scaled-down versions of large bars, and the gas response in nested bars differs profoundly from that in single bars. The gas flow in time-dependent nested-bar potentials is subject to dynamical constraints, such as conditions minimizing chaos. In order to decrease the fraction of chaotic orbits in the system, CR of the secondary bar must lie in the vicinity of the primary-bar ILR (Tagger et al. 1987; Pfenniger & Norman 1990), constraining  $\Omega_s$ . Such a dynamical configuration, in principle, poses a problem for uninterrupted gas inflow towards smaller radii: the gas flow is repelled from the small bar CR, because of the rim formed by the effective potential there. Shlosman et al. (1989) have argued, in essence, that it is the gas self-gravity that overcomes such repulsion by modifying the underlying potential. In fact, even in the limit of negligible self-gravity in the gas, the flow is capable of crossing the bar–bar interface, but not in a steady manner and only for a restricted range of azimuthal angles (Shlosman & Heller 2002).

To analyze the gas flow in nested bars, one can define the following three regions: *(i)* the primary-bar region (outside its ILR), *(ii)* the bar–bar interface (hereafter the *interface*) encompassing the outer ILR of the large bar and the outer part of the secondary bar, and *(iii)* the interior of the secondary bar. In the first region, the gas responds by forming a pair of large-scale shocks and flows inwards across the interface. The flow in the primary bar, outside the interface, is steady and the shock strength and shape are nearly independent of time. In the second region, the flow is time-dependent due to the perturbative effects of the secondary bar and changing background potential. The inflow proceeds on the average along the primary-bar minor axis, while an outflow (albeit at a smaller rate) is directed along its major axis. This happens because the inflow is driven mainly along the large-scale shocks penetrating the interface. At the same time the outflow is detected at angles which ‘avoid’ the large-scale shocks.



*Left:* Figure 3. Pattern of shock dissipation (left) and density evolution (right) in the central kpc, in the frame of reference of the primary bar (horizontal). Positions of the secondary bar and its length are indicated by a straight line. All rotation is counter-clockwise. Particles on the left have greater than average dissipation rate, given by the time derivative of the nonadiabatic component of internal energy. Note the sharply reduced dissipation in the innermost secondary bar and “limb brightening” enveloping it. Also visible are two dissipative systems associated with the shocks in the primary bar and with the trailing shocks in the secondary bar (Shlosman & Heller 2002). *Right:* Figure 4. Time evolution of the low-viscosity model: 2D SPH simulation in the background gravitational potential of a barred disk galaxy (shown face on). The gas response to the bar torquing is displayed in the primary-bar frame. The primary bar is horizontal and the gas rotation is counter-clockwise. Note a fast evolution after  $t \sim 150$ , when the secondary bar decouples and swings clockwise! The bar is “captured” again at  $t \sim 211$ . Time is given in units of dynamical time. This animation sequence and others are available in the online edition of Heller et al. (2001).

The gas, which is repelled by the secondary bar is found to enter large-scale shocks while still moving out, increases the mixing of material with different angular momenta. The net effect is an inflow across the CR of the secondary bar (Fig. 3 in Shlosman & Heller 2002). The inflow shows the beat frequency clearly identified with the secondary bar tumbling. The corresponding mass influx rate is of the order of  $0.3 M_{\text{gas},9} M_{\odot} \text{ yr}^{-1}$ , where  $M_{\text{gas},9}$  is the total gas mass in the disk in units of  $10^9 M_{\odot}$  within the CR of the large bar.

Crossing the bar interface, the gas falls towards the third region, the inner  $1/2$ – $1/3$  of the bar where the flow is very relaxed, with uniform dissipation (well below the maximum dissipation in the large-scale shocks), and no evidence for grand-design shocks. A “limb brightening” can be noted at the edge of the small bar revealing an enhanced density of above-average dissipating particles outside the oval-shaped central region, which results from the gas joining the bar from all azimuths. The pattern of shock dissipation in nested bars (Fig. 3) allows one to separate the incoming large-scale shocks from those driven by the secondary bar. Note that two systems of spiral shocks occur. The shapes of the shocks depend on the angle between the bars. These spiral shocks driven by the secondary bar may have observational counterparts.

A number of factors characterize the gas dynamics in the *decoupled* bars: (i) the time-dependent nature of the gravitational potential; (ii) the nonsteady gas injection into the secondary bar which proceeds through the primary shocks penetrating the bar–bar interface. This phenomenon is absent at the CR of the primary bars. Unstable orbits in the interface region preclude the secondary bars from extending to their CR (El-Zant & Shlosman 2002); (iii) a fast-tumbling secondary bar which prevents the secondary ILRs from forming. Even in the case of a long-lived decoupled phase secondary bars are not expected to slow down. The gas inflow across the interface and the resulting central concentration can speed-up the bar (Heller, Noguchi, & Shlosman 1993, unpublished). The low-Mach-number gas flow is well organized and capable of following these orbits with little dissipation. Non-linear orbit analysis reveals that, in the deep interior of the secondary bar, the  $x_1$  orbits have a mild ellipticity and no end-loops. This result is robust. No offset large-scale shocks form under these conditions.

With no ILRs in a large bar, the offset shocks weaken and recede to its major axis, becoming “centered,” but do not disappear completely (Athanasoula 1992). Only two examples of centered shocks have been found from more than a hundred bars. During the last decade only one more potential example has been added to this list (Athanasoula, private communication). It seems plausible that centered shocks are very rarely observed because they are so weak.

Knapen et al. (1995) have analyzed the shock dissipation in a self-consistent gravitational potential of “live” stars and gas *before* decoupling, when both bars tumble with the same pattern speeds, and when the gas self-gravity is accounted for. No offset shocks have been found in this configuration either.

We conclude that no large-scale shocks and consequently no offset dust lanes will form inside secondary bars, whether they are dynamically coupled or decoupled. The time-dependent, “anisotropic” gas inflow across the interface found here is a completely new phenomenon inherent to nested bars. The fate of the gas settling inside secondary bars cannot be decided without invoking its global self-gravity that will completely change the nature of the flow. Under the

observed conditions in numerical simulations (gas masses and surface densities) the gas self-gravity should exert a dominating effect on its evolution (section 4.2).

#### 4. Nested Bars: Dynamical Decoupling

Probably the most intriguing property of nested bars is their theoretically anticipated stage of a decoupling, when each bar exhibits a different pattern speed (Shlosman et al. 1989). Decoupling is indirectly supported by the observed random orientation of nested bars. In principle, the following options exist for secondary bar rotation. First, both bars corotate, being completely synchronized. This configuration of nearly orthogonal bars can be a precursor to the future decoupled phase or continue indefinitely. A simple explanation of this phenomenon lies in the existence two main families of periodic orbits in barred galaxies. The gas responding to the gravitational torques from the primary bar flows towards the center and encounters the region of  $x_2$  orbits, which it populates. The forming secondary bar may be further strengthened by the gas gravity, which drags stars into  $x_2$  orbits. The amount of gas accumulating in the ILR resonance region may be insufficient to cause the dynamical runaway.

Next, if the secondary bar forms via self-gravitational instability (in stellar or gaseous disks), it must spin in the direction of the primary bar with  $\Omega_s > \Omega_p$  (Shlosman et al. 1989; Friedli & Martinet 1993; Combes 1994; Heller & Shlosman 1994). The presence of gas appears to be imperative for this to occur. Both bars are dynamically *decoupled* and the angle between them is arbitrary. Lastly, the secondary bar can rotate in the opposite sense to the primary bar, resulting from merging (Sellwood & Merritt 1994). This appears to be a non-recurrent configuration.

Although above options make specific predictions verifiable observationally, the triggering mechanism(s) for decoupling require better understanding. The computational effort has so far gone into analyzing self-gravitating systems (e.g., Friedli 1999; Shlosman 1999). However, dynamical evolution proceeds beyond the formation of two coupled bars, even when gas self-gravity is neglected (Heller et al. 2001): partial or complete decoupling of a gaseous bar, depending on the degree of viscosity in the gas, can be triggered for a prolonged period of time (section 4.1). Both regimes are likely to be encountered in nature.

*4.1. Decoupling of Non-Self-Gravitating Bars.* The actual degree of viscosity in the ISM is largely unknown. Heller et al. (2001) have investigated the effect of viscosity on the gas settling in the ILR region of a single large-scale stellar bar. Using identical initial conditions, the non-self-gravitating gas was evolved by means of a 2D version of the SPH code (Heller & Shlosman 1994), or, alternatively, using the grid code ZEUS-2D, exhibiting similar results.

The most spectacular evolution occurred in the low-viscosity model, although all the models showed similar initial evolution, during which the gas accumulated in a double ring, corresponding roughly to two ILRs. In all the models the rings interact hydrodynamically and merge (Fig. 4). After merging, a single oval-shaped ring corotates with the primary bar, leading it by  $\phi_{\text{dec}}$ , the decoupling angle whose value depends on the gas viscosity. In all the models, the remaining ring becomes increasingly oval and barlike (Figs. 4, 5), its pattern speed changes abruptly, and it swings towards the primary bar, *against* the di-



rection of rotation. In the inertial frame, this forming gaseous bar spins in the same sense as the main bar, albeit with  $\Omega_s < \Omega_p$ , but in the primary-bar frame it tumbles in the retrograde direction! This is sustained for about 60 dynamical times,  $\sim 2\text{--}3 \times 10^9$  yr, until it is captured again by the primary potential. The shape of the decoupled bar and  $\Omega_s$  depend on bar orientation. The eccentricity,  $\epsilon$ , reaches a maximum when bars are aligned (Fig. 5). In standard and high-viscosity models, the secondary bar only librates about the primary bar.

The key to understanding this behavior lies in the distribution of gas particles with Jacobi energy,  $E_J$ . After merging the ring is positioned close to the energy where the transition from  $x_2$  to  $x_1$  (at the inner ILR) occurs. The exact value of this transition energy is model-dependent, but this is of no importance to the essence of the decoupling. The crucial difference between the models comes from (i) the position of the forming gaseous bar on the  $E_J$  axis after ring merging and (ii) the value of  $\phi_{\text{dec}}$ . We note that the role of viscosity here is fundamentally different from that in nearly axisymmetric potentials (planetary rings, galactic warps, etc.), where it acts to circularize the orbits.

As the gaseous bar forms at the angle  $\phi_{\text{dec}}$  to the primary bar, gravitational torques act to align the bars. In the low-viscosity model, gaseous bar resides on purely  $x_2$  orbits and, therefore, responds to the torque by speeding up its precession while being pulled backwards, until it is almost at right angles to the bar potential valley. The decoupling happens abruptly when  $\sim 1/2$  of the gas finds itself at  $E_J$  below the inner ILR. The absence of  $x_2$  orbits at these  $E_J$  means that the gas loses its stable orientation along the primary-bar minor axis. The gaseous bar has a much smaller  $\epsilon$  in the fourth quadrant than in the first. Such an asymmetry with respect to the primary-bar axis ensures that the torques from the primary bar are smaller in the fourth quadrant. But only for the least viscous model this becomes crucial, and the torques are unable to confine the bar oscillation, which continues for a full swing of  $2\pi$ . The nuclear bar is trapped again at  $\tau \sim 211$ , after few rotations with respect to the large-scale bar.

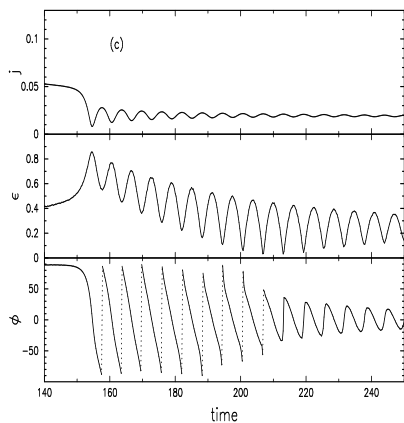


Figure 5. Low-viscosity model (see Fig. 4): evolution of total specific angular momentum  $j$  in the primary-bar frame of reference (*upper*), eccentricity  $\epsilon$  (*middle*), and position angle,  $\phi$ , of the line of apsides (*lower*) of the nuclear bar. The time unit is dynamical time. The angle  $\phi$  is shown between  $\pm\pi/2$  for presentation only, discontinuities are marked by vertical dotted lines. Decoupling of the nuclear bar exists between  $\tau \approx 150\text{--}211$  (Heller et al. 2001).

Correlation between  $\epsilon$  of the gaseous bar and its orientation can be tested observationally. Two additional effects should have observational consequences to decoupling and the periodic increase in  $\epsilon$ . First, the gas will cross the inner ILR on a dynamical timescale. Shlosman et al. (1989) pointed out that ILRs present a problem for radial gas inflow because the gas can stagnate there. A

solution was suggested in the form of a global self-gravitational instability in the nuclear ring or disk, which will generate gravitational torques in the gas, driving it further in. Recently Sellwood & Moore (1999) resurrected the idea that ILRs would “choke” the gas inflow. However, as we see here, even non-self-gravitating nuclear rings are prone to dynamical instability which drives the gas inwards. Moreover, the gas inflow is expected to be accompanied by star formation along the molecular bar, having a quasi-periodic, bursting character.

*4.2. Decoupling of Self-Gravitating Bars.* Gas self-gravity plays a crucial role in the formation and decoupling of bars, securing  $\Omega_s > \Omega_p$  (Shlosman et al. 1989; Shlosman 2001). Simulations which tackle this issue have been very limited so far. Friedli & Martinet (1993, and priv. communication) and Combes (1994) experienced difficulties in decoupling pure stellar or gaseous disks. The inner bar in this case is very transient, which may be a result of an insufficient number of particles. For a mixed system the decoupled stage is more prolonged. Simulations explicitly demonstrate the necessity for gas to be present, in addition to stars, and confirm that an increased central-mass concentration is important for the dynamical separation of the outer and inner parts. This can be achieved by moving the gas along the large-scale bar, accumulating it inside the ILR on the  $x_2$  orbits, modifying the local potential and forming a double ILR. The gravity of the gas settling into these orbits is sufficient to “drag” the stars along, but such a configuration still corotates with the primary bar. The ability of the gas to settle into the  $x_2$  orbits depends upon its sound speed and viscosity. When the gas is too viscous or hot, it will avoid the ILRs completely and remain on the  $x_1$  orbits aligned with the bar (Englmaier & Gerhard 1997; Englmaier & Shlosman 2000; Patsis & Athanassoula 2000). Moderately viscous gas will settle into the innermost  $x_2$  orbits. The evolution of nuclear regions in disks, therefore, depends on the (unknown) equation of state of the ISM. The inclusion of star formation in nuclear rings has already demonstrated how the resulting increase in viscosity leads to the mass transfer across the ILRs (Knapen et al. 1995).

Englmaier & Shlosman (Shlosman 2001) have accounted for gravitational effects in the gas. Ring evolution was similar to that described in 4.1, including the swing towards the primary bar. But this was followed by the rapid growth of *prograde* self-gravitating modes with  $m = 2$  and 4 with the pattern speed much larger than  $\Omega_p$ , resulting in an avalanche-type inflow. A model with the seed supermassive BH revealed that inflowing gas feeds the BH at peak rates, increasing its mass tenfold. A big unknown is the concurrent star formation, which was neglected in these simulations. Note, however, that the star formation has low efficiency and can hardly halt this runaway collapse toward the center.

## 5. Nested Bars at Higher Redshifts?

Although galactic disks show little evolution for  $z < 1$  (Le Fevre et al. 2000), at higher redshifts the situation is expected to change. Disk formation and stability should depend on halo shape and its cuspidity. Analysis of bar dynamics in cuspy axisymmetric halos has revealed their strong trend to brake (Debattista & Sellwood 2000) and the cusp leveling (Weinberg & Katz 2002). One should question the very existence of large-scale bars in this environment. Even if the cusps can be dissolved by the very same processes which form the disks (El-Zant,

Shlosman & Hoffman 2001), unless the halos are perfectly axisymmetric, they would impede growth of large bars (El-Zant & Shlosman 2002). Hence, first bars may be confined to within the central kpc of growing disks, at redshifts corresponding to galaxy formation epoch. The characteristic timescales, dynamical or secular, over which the disks acquire their present size are not known. One can conjecture that the formation of disks at large (on  $\sim 10$  kpc scale) can be decoupled from dynamics of central kpc, resulting in buildup of nested bars in the reverse order, i.e., from smaller to larger spatial scales. The observational verification of this scenario should probably wait for the *NGST* and is unrelated to the reported deficiency of large-scale bars for  $z \sim 0.5 - 0.8$  (e.g., Abraham et al. 1999) which may have an alternative explanation (Jogee et al. 2002).

## 6. Conclusions

The lifetime of nested bars is not clear at present and the configuration itself can be recurrent. The secondary bars can be responsible for accelerating dynamical and secular evolution within the central kpc, fueling stellar and nonstellar activity there, and driving the nuclear spiral arms. Their role in the formation and initial evolution of galactic disks is far from being understood. Simulations will clarify the issues related to nested bar formation and the role of self-gravitating gas in this process. Coupled with new observational techniques and instruments at longer wavelengths, they will shed light on the intricate evolution of central regions within the general context of cosmological evolution.

**Acknowledgments.** I am grateful to my collaborators Amr El-Zant, Peter Englmaier, Clayton Heller, Shardha Jogee, Johan Knapen, Seppo Laine and Reynier Peletier, and to my colleagues, too numerous to list here, for many in-depth discussions on this subject. This work is supported in part by NASA grants NAG 5-10823, HST GO-08123.01-97A, and WKU-522762-98-6.

## References

- Abraham, R.G., Merrifield, M.R., Ellis, R.S., Tanvir, N.R., & Brinchmann, J. 1999, *MNRAS*, 308, 569
- Athanassoula, E. 1992, *MNRAS*, 259, 345
- Athanassoula, E., & Martinet, L. 1980, *A&A*, 87, L10
- Buta, R., & Crocker, D.A. 1993, *AJ*, 105, 1344
- Combes, F. 1994, *Mass-Transfer Induced Activity in Galaxies*, ed. I. Shlosman (Cambridge: Cambridge University Press), p. 170
- Debattista, V.P., & Sellwood, J.A. 2000, *ApJ*, 543, 704
- de Vaucouleurs, G. 1974, in *IAU Symp. 58, The Formation and Dynamics of Galaxies*, ed. J.R. Shakeshaft (Dordrecht: Reidel), p. 335
- Devereux, N.A., Kenney, J.D.P., & Young, J.S. 1992, *AJ*, 103, 784
- El-Zant, A., & Shlosman, I. 2002, in preparation
- El-Zant, A., Shlosman, I., & Hoffman, Y. 2001, *ApJ*, 760, 636
- Englmaier, P., & Gerhard, O. 1997, *MNRAS*, 287, 57

- Englmaier, P., & Shlosman, I. 2000, *ApJ*, 528, 677
- Forbes, D.A., Kotilainen, J.K., & Moorwood, A.F.M. 1994, *ApJ*, 433, L13
- Friedli, D. 1999, *Evolution of Galaxies on Cosmological Timescales*, ed. J.E. Beckman & T. J. Mahoney, eds. (San Francisco: ASP). p. 88
- Friedli, D., & Martinet, L. 1993, *A&A*, 277, 2
- Heller, C.H., & Shlosman, I. 1994, *ApJ*, 424, 84
- Heller, C.H., Shlosman, I., & Englmaier, P. 2001, *ApJ*, 553, 661
- Ishizuki, S., Kawabe, R., Ishiguro, M., Okumura, S.K., & Morita, K.-I. 1990, *Nat*, 344, 224
- Jogee, S., Knapen, J.H., Laine, S., Shlosman, I., Scoville, N.Z., & Englmaier, P. 2002, *ApJ*, submitted
- Knapen, J.H., Shlosman, I., & Peletier, R.F. 2000, *ApJ*, 529, 93
- Knapen, J.H., Beckman, J.E., Heller, C.H., Shlosman, I., & de Jong, R.S. 1995, *ApJ*, 454, 623
- Kotilainen, J.K., Reunanen, J., Laine, S., & Ryder, S.D. 2000, *A&A*, 353, 834
- Laine, S., Shlosman, I., Knapen, J.H., & Peletier, R.F. 2002, *ApJ*, March 1, in press (astro-ph/0108029)
- Le Fevre, O., et al. 2000, *MNRAS*, 311, 565
- Maciejewski, W., Teuben, P.J., Sparke, L.S., & Stone, J.M. 2002, *MNRAS*, in press, astro-ph/0109431
- Maiolino, R., Alonso-Herrero, A., Anders, S., Quillen, A., Rieke, M.J., Rieke, G.H., & Tacconi-Garman, L.E. 2000, *ApJ*, 531, 219
- Martin, P. 1995, *AJ*, 109, 2428
- Martini, P., & Pogge, R.W. 1999, *AJ*, 118, 2646
- Mirabel, I.F., et al. 1999, *A&A*, 341, 667
- Mulchaey, J.S., & Regan, M.W. 1997, *ApJ*, 482, L135
- Patsis, P.A., & Athanassoula, E. 2000, *MNRAS*, 358, 45
- Pfenniger, D., & Norman, C.A. 1990, *ApJ*, 363, 391
- Regan, M.W., & Mulchaey, J.S. 1999, *AJ*, 117, 2676
- Sellwood, J.A., & Wilkinson, A. 1993, *Rep.Prog.Phys.*, 56, 173
- Sellwood, J.A., & Merritt, D. 1994, *ApJ*, 425, 530
- Sellwood, J.A., & Moore, E.M. 1999, *ApJ*, 510, 125
- Shaw, M.A., Combes, F., Axon, D.J., & Wright, G.S. 1993, *A&A*, 273, 31
- Shlosman, I. 1999, *Evolution of Galaxies on Cosmological Timescales*, ed. J.E. Beckman & T. J. Mahoney, (San Francisco: ASP), p. 100
- Shlosman, I. 2001, *The Central Kpc of Starbursts & AGNs*, ed. J.H. Knapen et al. (San Francisco: ASP), p. 55
- Shlosman, I., & Heller, C.H. 2002, *ApJ*, February 1, in press, (astro-ph/0109536)
- Shlosman, I., Frank, J., & Begelman, M.C. 1989, *Nat*, 338, 45
- Shlosman, I., Begelman, M.C., & Frank, J. 1990, *Nat.*, 345, 679
- Tagger, M., Sygnet, J.F., Athanassoula, E., & Pellat, R. 1987, *ApJ*, 318, L43
- Weinberg, M.D., & Katz, N. 2002, preprint, astro-ph/0110632